Scientific Research Publishing

Modern Research in Catalysis, 2017, 6, 30-46
http://www.scirp.org/journal/mrc
ISSN Online: 2168-4499
ISSN Print: 2168-4480

# An Investigation on Kinetics of Photo Catalysis, Characterization, Antibacterial and Antimitotic Property of Electrochemically Synthesized ZnS and $ZrS_2$/ZnS Nano Photocatalysts

**Hosaholalu Balakrishna Uma[1], Sannaiah Ananda[1*], Vittal Ravishankar Rai[2], Kiana Alasvand Zarasvand[2]**

[1]Department of Studies in Chemistry, University of Mysore, Mysuru, India
[2]Department of Studies in Microbiology, University of Mysore, Mysuru, India
Email: umapriyahb2015@gmail.com, *snananda@yahoo.com, raivittal@gmail.com, kianaalasvand@gmail.com

**How to cite this paper:** Uma, H.B., Ananda, S., Rai, V.R. and Zarasvand, K.A. (2017) An Investigation on Kinetics of Photo to Catalysis, Characterization, Antibacterial and Antimitotic Property of Electrochemically Synthesized ZnS and $ZrS_2$/ZnS Nano Photocatalysts. *Modern Research in Catalysis*, **6**, 30-46.
http://dx.doi.org/10.4236/mrc.2017.61003

**Received:** October 9, 2016
**Accepted:** January 19, 2017
**Published:** January 22, 2017



## Abstract

Zinc sulphide is one of the commercially important II-VI semiconductors having a wide band gap, rendering it a very attractive material for optical application especially in nanocrystalline form. Nanocomposites of ZnS and $ZrS_2$/ZnS were prepared by simple electrochemical method; their photocatalytic properties had been investigated. The structure, composition and optical property of the product were characterized by X-ray diffraction (XRD), FE-SEM (EDAX), UV-VIS and IR techniques. The UV-VIS spectra exhibited a blue-shift with respect to that of bulk material due to quantum confinement effect. Kinetics of photocatalytic degradation of Indigo Carmine dye has been studied. The photocatalytic decolourization of the dye follows first order kinetics. The antimitotic and antibacterial activity of these nanoparticles was investigated.

## Keywords

Electrochemical Synthesis, Bioluminescence, *Photobacterium leiognathi*, *Allium cepa*

## 1. Introduction

Over the past few decades, environmental problems associated with harmful organic pollutants in waste water are driving force for sustained fundamental and applied research in the area of environmental remediation [1]. Semiconductor-assisted photo catalysis has received considerable attention as a promising tool

for implementing the purification of waste water and hydrogen energy production [2]. Last two decades have witnessed a rapid advancement in various techniques for the fabrication of nanoparticles [3] [4]. Among the various semiconducting materials, ZnS is a wide-band gap semiconductor of 3.8 eV having luminescent properties and photocatalytic applications. ZnS is one of the II-VI semiconducting material finding application in Cathode ray tubes, IR windows, injection lasers, ultraviolet light-emitting diodes and flat panel displays [5] [6]. Doping of metal ions into ZnS can influence the performance of these photocatalysts. ZnS has been extensively studied with the aim of controlling the size, morphology and crystallinity in order to obtain desired physical properties [7] [8]. Many methods have been used to synthesize ZnS nanoparticles such as sol-gel, hydrothermal, solvothermal and mechanochemical methods. ZnS obtained by this techniques has a wide band gap of 4 - 4.6 eV [9]. An electrochemical procedure based on the dissolution of a metallic anode in a protic solvent, has been used to obtain nanoparticles ranging from 10 to 20 nm with reduced band gap [10] [11].

Zr is a transition metal mainly used as refractory and opacifier and in small amount as an alloying agent for its strong resistance to corrosion. Zirconium containing compounds are used in many biomedical applications, including dental implants and other restorative practices, knee and hip replacements, although Zr has no known biological role [12] [13] [14]. However, a few papers have been reported on photocatalytic and biological applications of Zirconium doped nanoparticles. Doping of Zr to ZnS is quite attractive, since the dissolution potential of Zr (−1.45 eV) is more negative than Zn (−0.7618 eV) and also the radius of $Zr^{4+}$ (0.86 Å) is almost similar to that of $Zn^{2+}$ (0.88 Å). Keeping in view, ZnS and $ZrS_2$/ZnS nanocomposites were fabricated by the novel electrochemical method and their catalytic effects on photodegradation of Indigo carmine dye and antibacterial activity using Gram negative bioluminescent *Photobacterium leiognathi* and antimitotic activity using *Allium cepa* have been reported here.

## 2. Experimental

### 2.1. Synthesis of ZnS Nanoparticles

Zinc Sulphide nanoparticles are synthesized electrochemically using Zinc and platinum electrodes as shown in **Figure 1**. The electrolytic cell consisting of 0.5

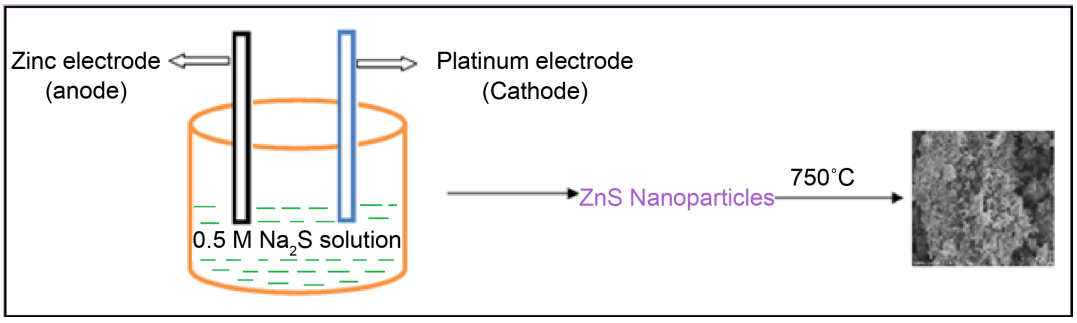


**Figure 1.** Diagrammatic representation of electrochemical formation of ZnS nanoparticles.

M aqueous $Na_2S$ solution and electrodes are separated by 1 cm. The experiment was run for 3 hrs with continuous stirring using 30 mA current and a potential of 20 V. During the electrolysis Zinc electrode acts as anode starts to dissolve and gives Zinc ions which are electrochemically reacted with sulphide ions furnished by $Na_2S$ to give ZnS nanoparticles. The obtained nanoparticles are washed repeatedly with distilled water till complete removal of Sodium Sulphide, centrifuged and calcinated at 750˚C for 2 hrs to remove Sodium and hydroxide impurities.

## 2.2. Synthesis of $ZrS_2/ZnS$ Nanoparticles

The experimental set up is similar to synthesis of ZnS. Here Zinc, platinum and Zirconium electrodes were used. The rate of electrochemical reaction is not same for $Zr^{4+}$ and $Zn^{2+}$, as the redox potential of $Zr^{4+}$ and $Zn^{2+}$ are different. Since the dissolution potential of Zr (−1.45 eV) is more negative than Zn (−0.7618 eV), formation of $ZrS_2$ takes place in competition with ZnS. The mechanism of electrochemical formation is as follows:

$$\mathrm{Zn} \rightleftharpoons \mathrm{Zn}^{2+} + 2e^-$$

$$\mathrm{Na_2S} \rightarrow 2\mathrm{Na}^+ + \mathrm{S}^{2-}$$

$$2\mathrm{Na}^+ + 2e^- \rightarrow 2\mathrm{Na}\left(\text{at Pt } e^- de\right)$$

$$\mathrm{Zn}^{2+} + \mathrm{S}^{2-} \rightleftharpoons \mathrm{ZnS}$$

$$\mathrm{Zr}^{4+} + 2\mathrm{S}^{2-} \rightleftharpoons \mathrm{ZrS_2}$$

**Scheme 1.** Mechanism of electrochemical formation of $ZrS_2$/ZnS nanocomposite.

## 2.3. Determination of Photocatalytic Activities

The photo reactivity of nanocatalysts are influenced by variables such as the dopant, pH of solution, dosage of photo catalyst, concentration of dye and exposure to different source of light viz., sunlight and UV light [15] [16]. Indigo carmine dye (Molecular formula: $C_{16}H_8O_8N_2S_2$, Molecular weight: 466.16, $\lambda_{max}$ = 610 nm) solution was prepared by dissolving in distilled water. This solution was used as test contaminant for evaluating photocatalytic activities. To assess the photocatalytic efficiency of the prepared nanoparticles, photodegradation experiments were carried out using different concentration of Indigo carmine dye as substrate and different concentrations of ZnS and $ZrS_2/ZnS$ as catalyst. A calculated amount of catalyst was added to the dye solution, stirred in dark for 1 min to establish adsorption/ desorption equilibrium between dye and nanoparticles and then illuminated under 8 W UV source to induce a photoche- mical reaction. Aliquots were taken at an interval of 2 min (in case of ZnS) and 10/15 min (in case of $ZrS_2/ZnS$) and percent transmittance was determined.

The adsorption and photocatalytic conversion (g%) was calculated as follows [17]:

$$\text{COD} = \frac{8000\left(\text{vol of FAS in blank} - \text{vol of FAS in dye soln}\right)\ \text{normality of FAS}}{\text{Sample volume}}.$$

The mineralization of dye was measured by the decrease of chemical oxygen demand (COD) of the solution. The COD was measured according to the standard dichromate titration method [18] [19]. The mineralization efficiency of dye was estimated by the following expression:

$$\%\ \text{efficiency} = \frac{\text{Initial COD} - \text{Final COD}}{\text{Initial COD}} \times 100.$$

The decrease in COD (mg/l) and increase in % $T$ of the dye solution with colour removal was observed as follows:

$$\text{ZnS nanoparticles} > \text{ZrS}_2/\text{ZnS nanoparticles}.$$

The mechanism of photodegradation can be represented as follows [20] [21].

$$\begin{aligned}
\text{Np} + h\nu &\rightarrow e^- + h^+ \\
h^+ + \text{H}_2\text{O} &\rightarrow \text{OH}\cdot + h^+ \\
h^+ + \text{OH}^- &\rightarrow \text{OH}\cdot \\
e^- + \text{O}_2 &\rightarrow \text{O}_2^- \\
\text{O}_2^- + \text{H}_2\text{O} &\rightarrow \text{HO}_2^{\bullet} + \text{OH}\cdot \\
\text{HO}_2^{\bullet} + \text{H}_2\text{O} &\rightarrow \text{OH}\cdot + \text{H}_2\text{O} \\
\text{H}_2\text{O}_2 &\rightarrow 2\text{OH}\cdot \\
\text{OH}\cdot + \text{IC} &\rightarrow \text{Intermediate products} \\
&\rightarrow \text{Degradation products} \\
\text{O}_2^- + \text{IC} &\rightarrow \text{Intermediate products} \\
&\rightarrow \text{CO}_2, \text{H}_2\text{O}, \text{NH}_3 \text{ and other degradation products}
\end{aligned}$$

**Scheme 2.** Mechanism of dye degradation by OH radical.

## 3. Results and Discussion

### 3.1. X-Ray Diffraction

The XRD pattern of synthesized ZnS and $\text{ZrS}_2/\text{ZnS}$ nanoparticles are shown in **Figure 2**. The XRD for ZnS shows three main diffraction peaks at $2\theta$ values 31.61, 34.28 and 36.08. The obtained peak positions correspond to Zinc blended type patterns and the XRD pattern is well matched with standard cubic ZnS [6]. The XRD of $ZrS_2$/ZnS nanoparticles are compared with ZnS nanoparticles and are as follows. From the XRD data it is evident that no much change in the position of diffraction peaks were observed compared to ZnS nanoparticles. A possible reason could be that $Zr^{4+}$ entered into the crystal lattice of ZnS and suppress the growth of ZnS crystals, because radius of $Zr^{4+}$ (0.86 Å) smaller than that of $Zn^{2+}$ (0.88 Å) and Zr substitutes Zn in the lattice. The slight change of lattice parameters of $\text{ZrS}_2/\text{ZnS}$ also proved that the Zr ions were incorporated into the ZnS lattice.

From the XRD data the cell parameters are calculated for ZnS nanoparticles and it is found to be $a = b \neq c$ ($a$ = 8.483 Å, $b$ = 8.483 Å and $c$ = 9.957 Å) and

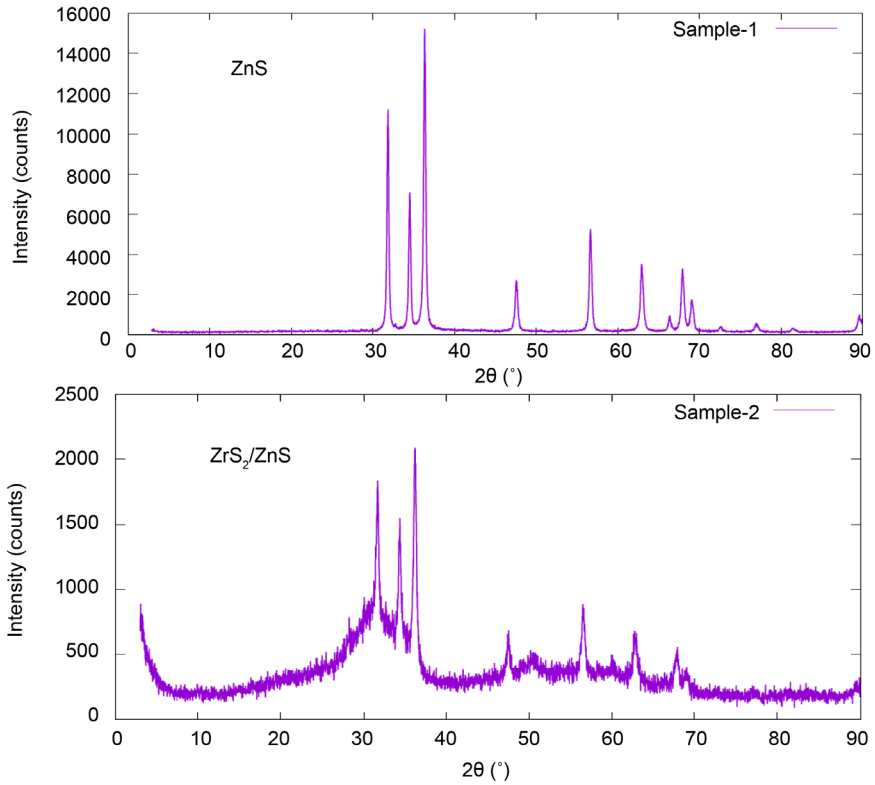


**Figure 2.** XRD patterns of ZnS and $ZrS_2$/ZnS nanoparticles.

$\alpha = \beta = \gamma = 90^{\circ}$. Accordingly, ZnS nanoparticles belong to Tetragonal crystal system. Using XRD data, the cell parameters calculated for $ZrS_2/ZnS$ nanoparticles are found to be $a = b \neq c$ ($a$ = 6.900 Å, $b$ = 6.900 Å and $c$ = 9.806 Å) and $\alpha = \beta = \gamma = 90^{\circ}$. Accordingly, $ZrS_2/ZnS$ nanoparticles belong to Tetragonal crystal system. The average crystallite size was calculated using Williamson-Hall plot [22] and it was found to be 57.2 nm for ZnS and 43.8 nm for $ZrS_2/ZnS$ nanoparticles. The angle strain is 3.46 × $10^{-2}$ for ZnS and 7.59 × $10^{-4}$ for $ZrS_2/ZnS$ nanocomposite.

## 3.2. Optical Absorption Spectra

The UV-Visible spectrum of ZnS and $ZrS_2/ZnS$ nanoparticles (**Figure 3**) over the range 200 - 600 nm showed that the synthesized nanoparticles are photoactive under UV light radiation. ZnS nanoparticles showed three absorption peaks where as $ZrS_2/ZnS$ nanoparticles showed two peaks in the UV region. There is no absorption peak in the visible region. The band gaps of the samples are calculated using Tauc's plot [23] [24] and was found to be 2.7 eV for ZnS and 3.9 eV for $ZrS_2/ZnS$ nanoparticles as shown in **Figure 4**. The obtained band gap value of ZnS nanoparticle is lower than that of the bulk value of ZnS (3.68 eV). This blue shift of the band gap of ZnS nanoparticle occurs due to quantum confinement effect [25]. The band gap of $ZrS_2/ZnS$ is very much higher than that of ZnS. This supports lower photocatalytic efficiency of $ZrS_2/ZnS$ nano particles compared to ZnS nanoparticles.

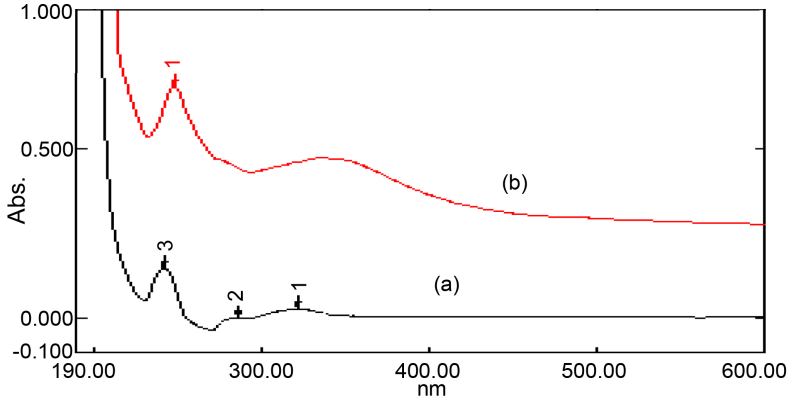


**Figure 3.** UV-Visible spectra of (a) ZnS and (b) $ZrS_2$/ZnS nanoparticles.

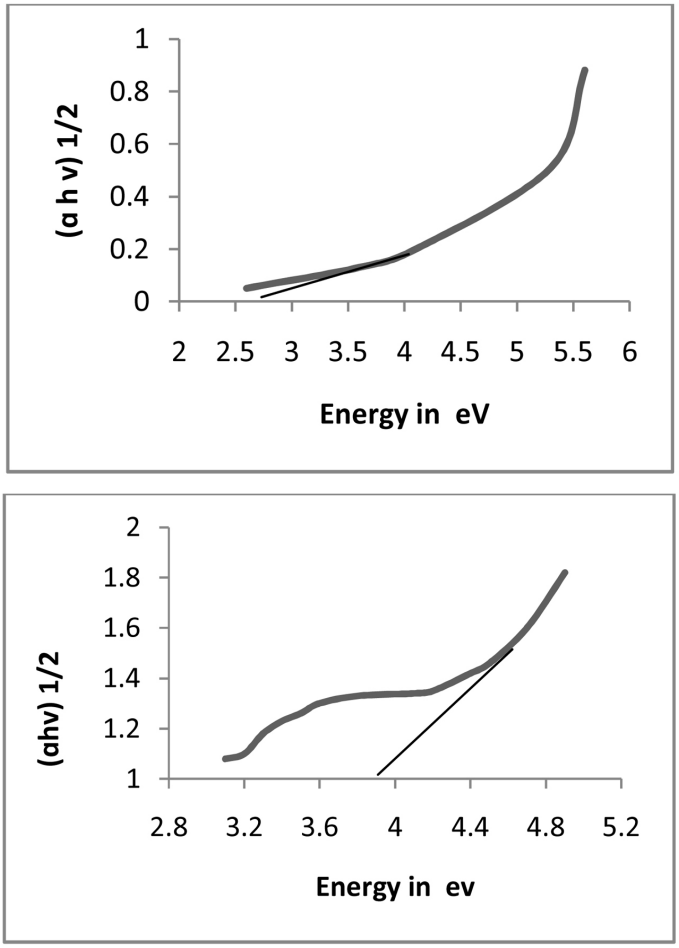


**Figure 4.** Tauc's plot of ZnS and $ZrS_2$/ZnS nanoparticles.

### 3.3. EDX of ZnS and $ZrS_2$/ZnS Nanoparticles

The EDAX analysis confirmed the presence of Zinc and Sulphur in ZnS and Zirconium, Zinc and Sulphur in $ZrS_2$/ZnS nanoparticles (**Figure 5** and **Figure 6**). The surface morphology of ZnS and $ZrS_2$/ZnS nanoparticles was observed by FE-SEM analysis. The SEM images showed that the synthesized nanoparticles consisted of agglomerated particles (**Figure 7**).

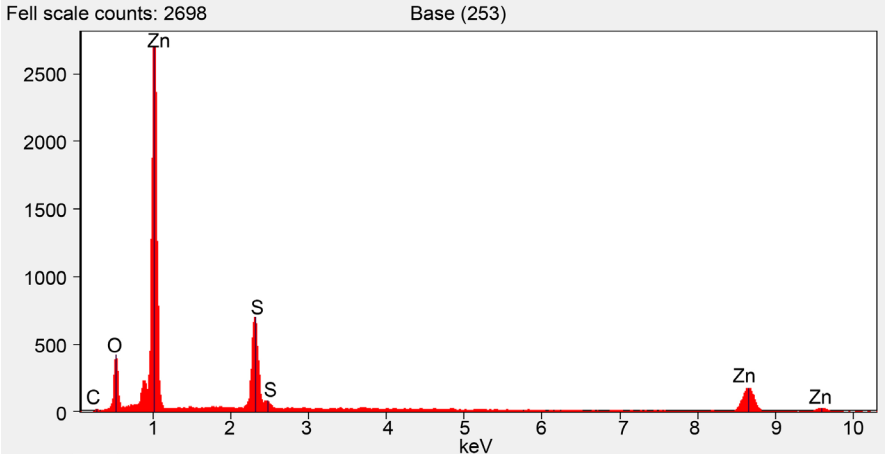


**Figure 5.** EDAX for ZnS nanoparticles.

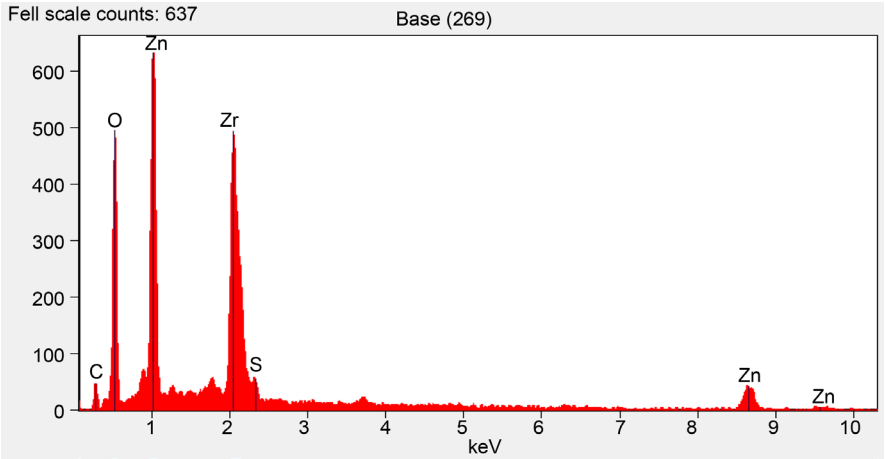


**Figure 6.** EDAX for $ZrS_2$/ZnS nanoparticles.

## 3.4. Photo Catalytic Degradation of Indigo Carmine Dye and COD Measurements

### 3.4.1. Effect of Concentration of Dye

To ensure the optimum dye concentration, photodegradation is carried out with different concentration of Indigo carmine with constant weight of catalyst (**Table 1** and **Figure 8**). As the optimum concentration of catalyst for ZnS nano particle is 0.02 g, keeping this as standard the same amount of $ZrS_2$/ZnS nanopartilce is taken for comparision in the further work. Beyond the optimum dye concentration, as the initial concentration of dye increases, the degradation efficiency reduces. The possible reason is that, as initial concentration of dye is increased, more dye molecules are adsorbed onto the surface of the catalyst. But the adsorbed dye molecules are not degraded immediately because the intensity of the light and the amount of catalyst is constant and also the light penetration is less. Also with increase in dye concentration, the solution becomes more intense coloured and the path length of the photons entering the solution is decreased thereby fewer photons reached the catalyst surface [17]. Hence there will be reduction in the production of ROS species like hydroxyl and superoxide

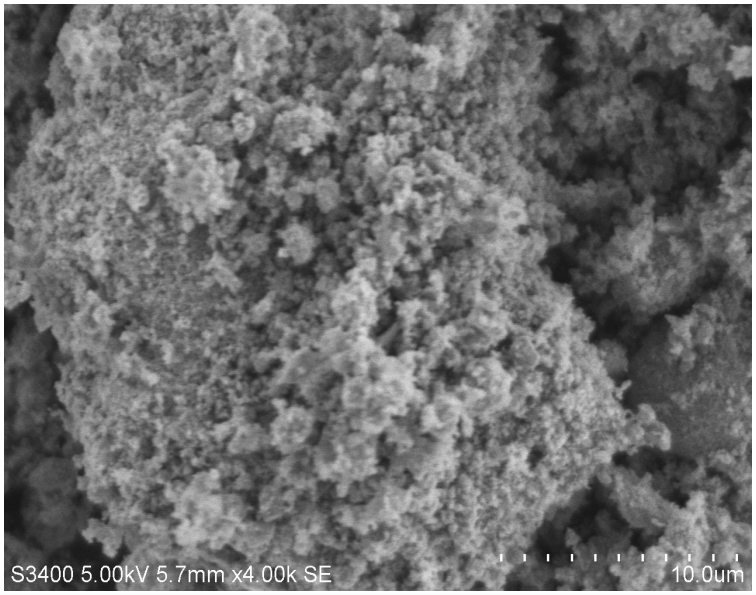


(a)

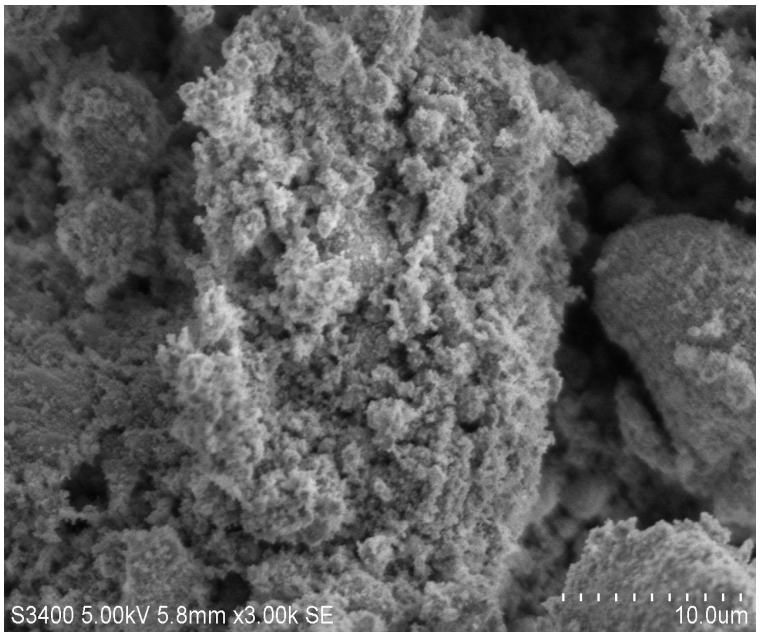


(b)

**Figure 7.** SEM micrographs of (a) ZnS and (b) $ZrS_2$/ZnS nanoparticles.

radicals [26].

### 3.4.2. Effect of Catalyst Loading

The experiments were performed by taking different amount of catalyst varrying from 0.02 to 0.06 g in order to study the effect of catalyst loading (**Table 2** and **Figure 9**). Photocatalytic rate initially increases with catalyst loading and then decreases at high values because of light scattering and screening effects [17] [27]. The tendency toward agglomeration also increases at high solid concentration, resulting in a reduction in the surface area available for light absorption and a decrease in photocatalytic degradation rate. The number of active sites in

**Table 1.** Effect of concentration of dye on the rate of degradation.

| Catalyst 0.02 g | Concentration of dye (M) | k·sec$^{-1}$ | Time taken for complete degradation (min) | COD values in mg·L$^{-1}$ | | Degradation efficiency % |
|---|---|---|---|---|---|---|
| | | | | Before degradation | After degradation | |
| Zinc sulphide | $0.1 \times 10^{-4}$ | $3.38 \times 10^{-4}$ | 13 | 304 | 48 | 84.21 |
| | $0.2 \times 10^{-4}$ | $5.11 \times 10^{-4}$ | 22 | 352 | 16 | 95.45 |
| | $0.3 \times 10^{-4}$ | $4.47 \times 10^{-4}$ | 82 | 360 | 64 | 82.22 |
| $ZrS_2/ZnS$ | $0.1 \times 10^{-4}$ | $3.41 \times 10^{-5}$ | 150 | 240 | 32 | 86.66 |
| | $0.2 \times 10^{-4}$ | $4.35 \times 10^{-5}$ | 315 | 432 | 48 | 88.88 |
| | $0.3 \times 10^{-4}$ | $6.39 \times 10^{-5}$ | 485 | 320 | 64 | 80.00 |

**Table 2.** Effect of catalyst loading on the rate of photo-degradation.

| Nano particle | Amount of catalyst/20ml | k·sec$^{-1}$ | Time taken for complete degradation (min) | COD values in mg/L | | Degradation efficiency % |
|---|---|---|---|---|---|---|
| | | | | Before degradation | After degradation | |
| Commercial ZnS | 0.02 g | $1.5 \times 10^{-4}$ | 92 | 352 | 288 | 18.18 |
| Zinc sulphide | 0.02 g | $14.04 \times 10^{-4}$ | 22 | 352 | 16 | 95.45 |
| | 0.04 g | $17.13 \times 10^{-4}$ | 22 | 352 | 16 | 95.45 |
| | 0.06 g | $12.95 \times 10^{-4}$ | 22 | 352 | 16 | 95.45 |
| $ZrS_2/ZnS$ | 0.02 g | $4.93 \times 10^{-5}$ | 210 | 192 | 32 | 83.33 |
| | 0.04 g | $7.67 \times 10^{-5}$ | 150 | 192 | 64 | 66.66 |
| | 0.06 g | $6.39 \times 10^{-5}$ | 130 | 192 | 96 | 50.00 |

solution will increase with catalyst loading, a point appears to be reached where light penetration is compromised because of excessive particle concentration [28]. A further increase in catalyst loading beyond the optimum will result in non-uniform light intensity distribution, so that the reaction rate would indeed be lower with increased catalyst dosage.

### 3.4.3. Effect of Temperature

Temperature is one of the important factor which effects the rate of photo-degradation. Increase of temperature is an indication of slighter increase in the rate of photodegradation as raise in temperature results in number of effective collisions leading to higher rate of reaction. However, the photodegradation efficiency is not much affected (**Table 3** and **Figure 10**).

### 3.4.4. Reuse of Catalyst

The possibility of reusing the photocatalyst was tested to see the cost effectiveness of the method used. After degradation of the dye, the dye solution was kept overnight and then the supernatant liquid was decanted. The photocatalyst was thoroughly washed with double distilled water and then reused for the photodegradation by taking fresh IC dye solution. The reuse sample has shown almost same degradation efficiency compared to the fresh samples (**Table 4** and

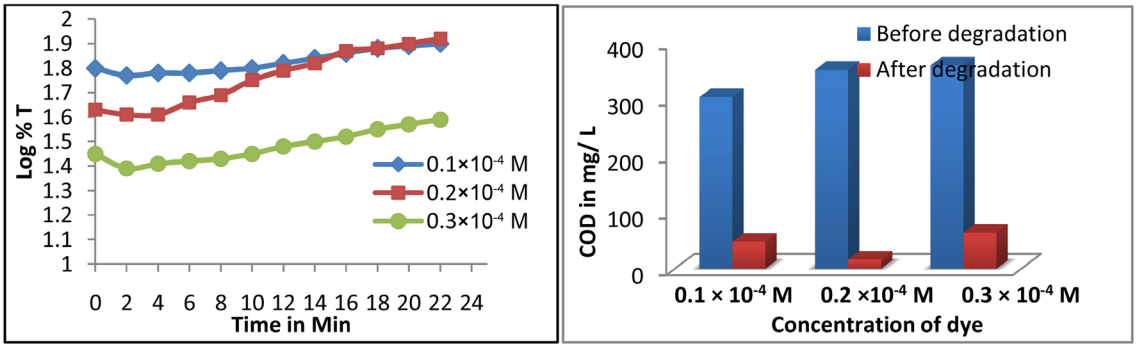


(a)

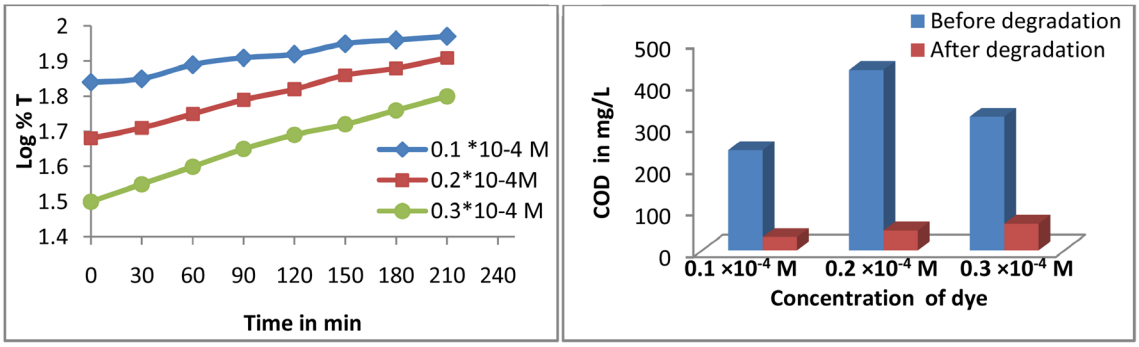


(b)

**Figure 8.** Plot of log % T vs. time with respect to different initial concentration of dye and COD values in case of (a) ZnS and (b) $ZrS_2$/ZnS nanoparticles.

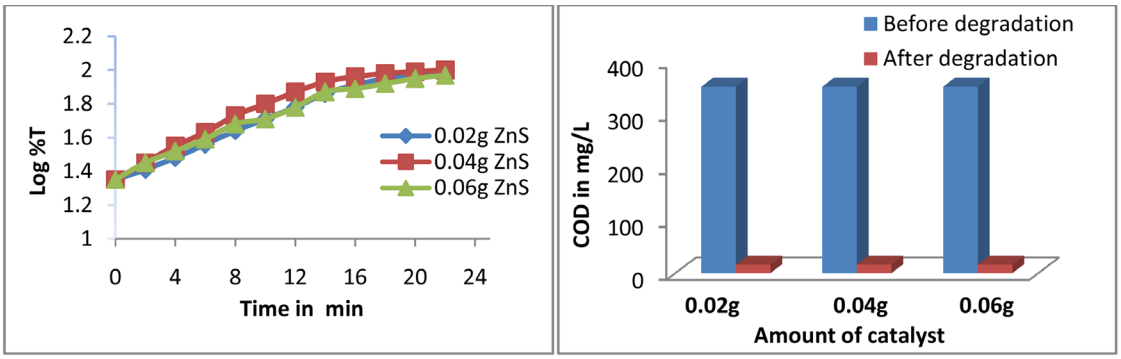


(a)

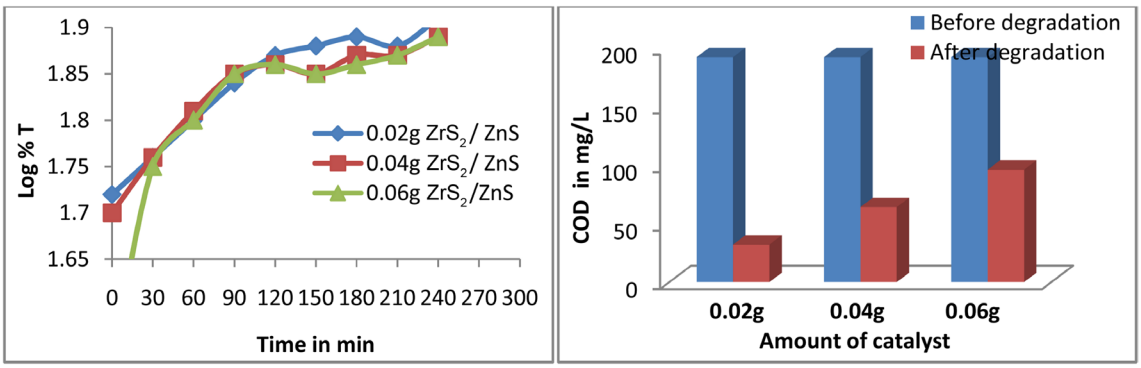


(b)

**Figure 9.** Plot of log % T vs. time with respect to catalyst loading and COD values in case of (a) ZnS and (b) $ZrS_2$/ZnS nanoparticles.

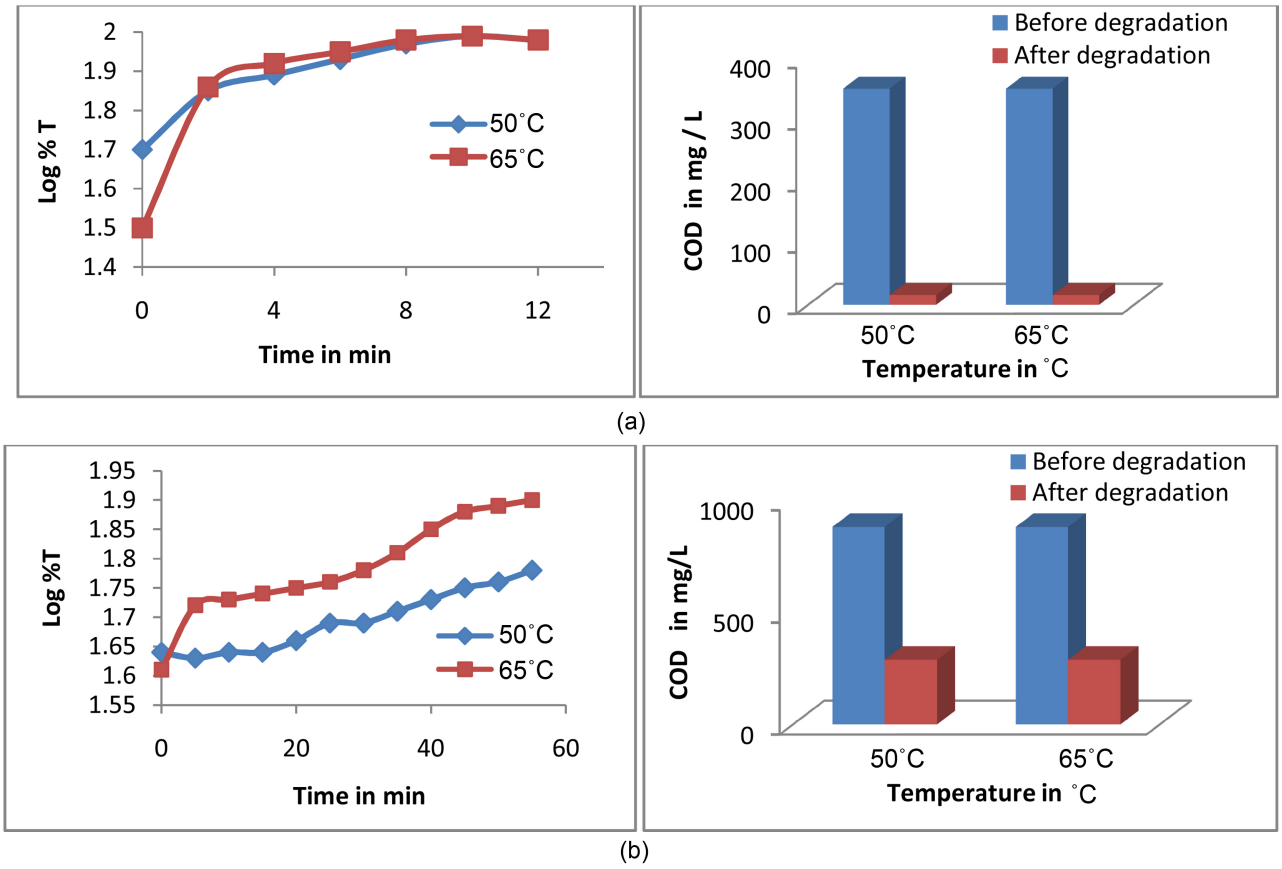


**Figure 10.** Plot of log % T vs. time with respect to temperature in case of (a) ZnS and (b) $ZrS_2$/ZnS nanoparticles.

**Table 3.** Effect of temperature on degradation of dye.

| Catalyst 0.02 g | Temp ˚C | Concentration of dye (M) | k·sec$^{-1}$ | Time taken for complete degradation (min) | COD values in mg/L | | Degradation efficiency % |
|---|---|---|---|---|---|---|---|
| | | | | | Before degradation | After degradation | |
| ZnS | 50 | $0.2 \times 10^{-4}$ | $13.5 \times 10^{-4}$ | 10 | 352 | 16 | 95.45 |
| | 65 | $0.2 \times 10^{-4}$ | $15 \times 10^{-4}$ | 12 | 352 | 16 | 95.45 |
| $ZrS_2$/ZnS | 50 | $0.2 \times 10^{-4}$ | $11.51 \times 10^{-5}$ | 110 | 880 | 288 | 67.27 |
| | 65 | $0.2 \times 10^{-4}$ | $8.25 \times 10^{-5}$ | 90 | 880 | 288 | 67.27 |

**Table 4.** Efficiency of catalyst in second use.

| Catalyst 0.02 g | Concentration of dye (M) | k·sec$^{-1}$ | Time taken for complete degradation (min) | COD values in mg/L | | Degradation efficiency % |
|---|---|---|---|---|---|---|
| | | | | Before degradation | After degradation | |
| ZnS | $0.2 \times 10^{-4}$ | $1.34 \times 10^{-4}$ | 130 | 352 | 16 | 95.4 |
| $ZrS_2$/ZnS | $0.2 \times 10^{-4}$ | $5.29 \times 10^{-5}$ | 290 | 352 | 64 | 81.81 |

Figure 11), while an obviously decrease in photoactivity was noticed with the reuse cycles [29]. This indicates the nano samples can be regenerated and reused

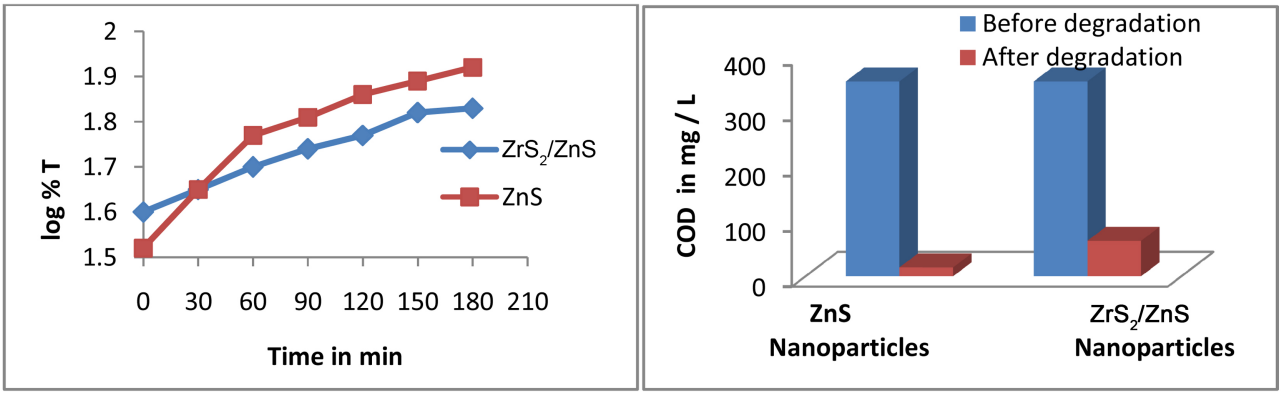


**Figure 11.** Plot of log % T vs. time with respect to reuse of catalyst and COD values in case of ZnS and $ZrS_2$/ZnS nanoparticles.

with very low or significance change in the efficiency. An obviously decrease in rate of reaction was observed with the second use of catalyst. Reuse cycles might cause the aggregation of photocatalyst and the decrease in specific surface area and the losses of catalyst, resulting in a loss of catalytic activity [30].

## 4. Biological Activities

### 4.1. Antibacterial Activity

#### 4.1.1. Bacterial Growth Condition

The Gram negative bioluminescent *Photobacterium leiognathi* (accession number: KM434234), isolated from coastal area of Goa, were used in this study. Bacteria were grown in nutrient broth (NB) containing 3% sodium chloride with aeration at 25˚C for 24 h. 10 µl of the overnight culture was inoculated into 100 ml of nutrient broth and incubated under same condition until the $OD_{600}$ reaches 0.5 (approximately 12 hours) as at this OD bacteria were emitting the maximum amount of light.

#### 4.1.2. Reagents

1 mg/ml stock solution nanoparticle (NPs) was prepared in sterile distilled water. To disperse the NPs, the suspension was sonicated before use. Later NPs dilutions were prepared in sterile broth. As these solutions are later inoculated with an equal amount of bacteria in broth, the dilutions are prepared at concentration twice the desired final concentration.

#### 4.1.3. Minimum Inhibitory Concentration (MIC) Assay

Broth microdilution technique has been used to determine the MIC of nanoparticle. For this purpose, two fold serial dilutions of the compound ranging from 500 to 0.4 µg/ml were performed in 96-well white microtiter plate. Initially 100 µl of bacterial inoculums was placed into the wells of the plate and later each well seeded with 100 µl of nanoparticle dilutions. Bacterial luminescent intensity was measured using a luminometer after 6 h incubation at 25˚C with 150 rpm shaking. In addition to the NP-treated well, each plate had untreated bacterial culture as control. Sterile broth containing NP and sterile broth also served as blank for the test and control respectively. NP efficacy was calculated from the

blanks, control and treated luminescence values on a plate.

$$\text{Percentage of inhibition} = \left[(C-B_1)-(T-B_2)/(C-B_1)\right]*100$$

where $B_1$ denotes the average luminescence for sterile broth, $B_2$ denotes the average luminescence for sterile broth containing NP, $C$ denotes the average luminescence for control and $T$ denotes the average luminescence for treated wells.

#### 4.1.4. Result and Discussion

The MIC is defined as the lowest concentration of NPs that inhibits the growth of a microorganism. The percentage of inhibition for ZnS and $ZrS_2/ZnS$ has showed in Table 5 and Figure 12. The MIC value for ZnS and $ZrS_2/ZnS$ is 500 and 15.6 µg/ ml respectively. These results indicate that the $ZrS_2/ZnS$ has higher antimicrobial activity than zinc sulphide.

### 4.2. Antimitotic Activity

The antimitotic activities of synthesized nanoparticles were determined by onion root tip method. *Allium cepa* has been used to evaluate the antimitotic activity of synthesized ZnS and $ZrS_2/ZnS$ nanoparticles. The results of antimitotic activity are given in Table 6 and the percentage inhibition of cell division by ZnS and $ZrS_2/ZnS$ nanoparticles comparative to control is given in Figures 13(a)-(d). Onion roots in ZnS and $ZrS_2/ZnS$ of concentration (25, 50 and 75 ppm)

Table 5. Inhibition of bacterial growth at different concentrations of nanoparticles (µg/ml).

| Np Concentration (µg/ml) | | 500 | 250 | 125 | 62.5 | 31.25 | 15.6 | 7.8 | 3.9 | 1.9 | 0.97 | 0.48 |
|---|---|---|---|---|---|---|---|---|---|---|---|---|
| % of inhibition | $ZrS_2/ZnS$ | 148 | 140 | 130 | 127 | 110 | 100 | 75 | 74 | 72 | 70 | 15 |
| | ZnS | 124 | 86 | 69 | 54 | 37 | 35 | 33 | 31 | 20 | 16 | 5 |

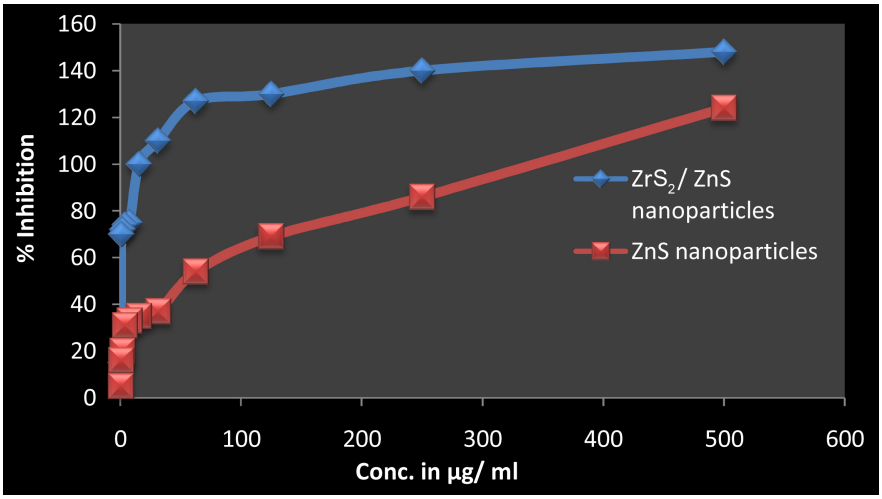


Figure 12. Plot of % Inhibition vs. Conc. in µg/ml with respect to ZnS and $ZrS_2/ZnS$ Nanoparticles.

**Table 6.** Antimitotic activity results of ZnS and $ZrS_2$/ZnS nanoparticles.

| Compound | Conc. in ppm | % Dividing cells | | | % Dividing Cells compared to control | | | % Inhibition compared to control | | |
|---|---|---|---|---|---|---|---|---|---|---|
| | | 12 hrs | 18 hrs | 24 hrs | 12 hrs | 18 hrs | 24 hrs | 12 hrs | 18 hrs | 24 hrs |
| Control | SDW | 67.03 | 74.27 | 71.24 | 0.00 | 0.00 | 0.00 | 00.00 | 0.00 | 0.00 |
| ZnS | 25 | 43.21 | 33.23 | 36.79 | 64.46 | 44.74 | 51.63 | 35.53 | 55.25 | 48.36 |
| | 50 | 42.41 | 30.71 | 33.14 | 63.26 | 41.34 | 46.52 | 36.73 | 58.65 | 53.47 |
| | 75 | 39.81 | 32.13 | 27.21 | 59.39 | 43.25 | 38.19 | 40.60 | 56.74 | 61.80 |
| $ZrS_2$/ZnS | 25 | 30.88 | 29.20 | 32.63 | 46.07 | 39.31 | 45.80 | 53.92 | 60.68 | 54.19 |
| | 50 | 27.41 | 30.13 | 33.26 | 40.89 | 40.56 | 46.69 | 59.10 | 59.43 | 53.30 |
| | 75 | 28.58 | 29.71 | 29.11 | 42.63 | 40.00 | 40.86 | 57.36 | 59.99 | 59.13 |

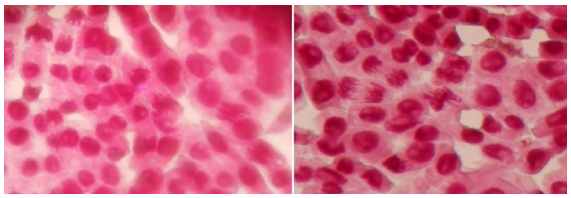

(a)

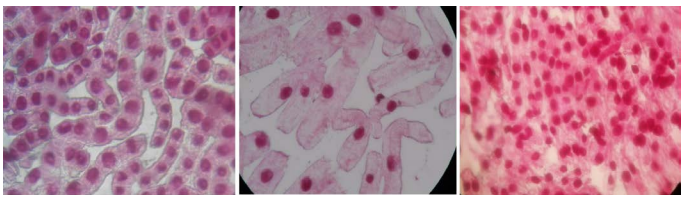

(b)

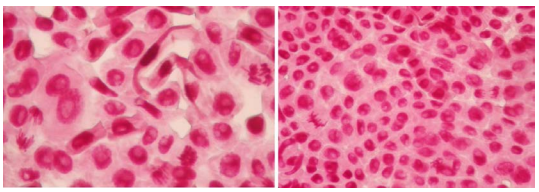

(c)

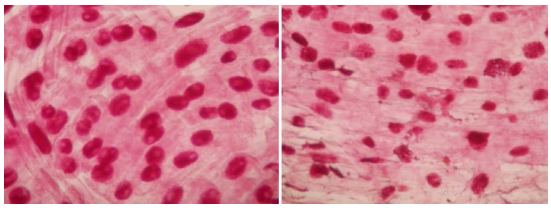

(d)

**Figure 13.** (a) Various stages of cell divisions seen under 40× microscopic field with normal cell division stages in control (SDW) treated groups. (b) Cells seen after 12 hours of treatment and observed under A: 40× with less stages of cell divisions, B: seen under oil immersion, there is no any further stages of cell divisions. (c) Cells seen after 18 hours of treatment and observed under A: 40× with very few stages (prophase, late anaphase and early anaphase) of cell divisions, B: seen under 40× microscopic fields with only metaphase. (d) Cells seen after 24 hours of treatment observed under 40 × microscopic views with very less cell divisions showing chromosomal aberrations, nuclear disintegration and initiation of cellular autolysis with formation of ghost cells.

at different time duration (12, 18 and 24 hrs) exhibited changes in chromosomes and shape of the cells with elongated appearance. The change in chromosomes and cellular morphology were achieved in increasing time and concentration. ZnS and $ZrS_2/ZnS$ nanoparticles showed good inhibitory effect by inhibiting the cell growth.

From the above observations, the partial-c-mitosis, full-c-mitosis with partial functional spindles and comparatively normal mitotic cells phases were noticed in various cells of the same root tip between 12 - 24 hrs time duration. Therefore, the antimitotic ability of ZnS and $ZrS_2/ZnS$ was remarkable in controlling the cell division and acts as potent antimitotic agents.

## 5. Conclusion

In this study, we have reported the synthesis of ZnS and $ZrS_2/ZnS$ nanoparticles by novel electrochemical method which is simple, cost effective and eco-friendly method. The photo degradation by these semiconductors offers a green technology for the removal of hazardous compounds present in waste water and industrial effluents. The kinetics of degradation of Indigo carmine has been studied. The complete degradation reaction was confirmed by conducting COD experiment. The synthesized nanoparticles are capable of entering into the *Allium cepa* cell and bacterial cell, therefore, inhibit the cell growth and hence confirm the biological activity as a potent antimitotic and antimicrobial agents. Moreover, $ZrS_2/ZnS$ nanoparticles have less photo catalytic activity compared with ZnS nanoparticles towards photodegradation. The presence of Zr suppresses the rate of photo-catalytic activity. ZnS nanoparticles are very good photocatalyst compared with $ZrS_2/ZnS$ nanocomposite. Hence, $ZrS_2/ZnS$ nanocomposite can be used to block UV radiation and can be used in the preparation of cosmetics. The degradation efficiency is ~95% in case of ZnS where as 83% in $ZrS_2/ZnS$ nanocomposites.

## Acknowledgements

This work has been supported by University of Mysore, Mysuru and the Author Uma, H. B. is thankful to UGC, New Delhi for providing financial assistance through BSR meritorious fellowship.

## Competing Interests

Authors have declared that no competing interests exist.

## References

[1] Zhang, L., Wong, K.-H., Chen, Z., Yu, J.C., Zhao, J., Hu, C., Chan, C.Y. and Wong, P.K. (2009) AgBr-Ag-$Bi_2WO_6$ Nanojunction System: A Novel and Efficient Photocatalyst with Double Visible-Light Active Components. *Applied Catalysis A*: *General*, **363**, 221-229. https://doi.org/10.1016/j.apcata.2009.05.028

[2] Therese, G.H.A. and Kamath, P.V. (2000) Electrochemical Synthesis of Metal Oxides and Hydroxides. *Chemistry of Materials*, **12**, 1195-1204. https://doi.org/10.1021/cm990447a

[3] Senapati, U.S., Jha, D.K. and Sarkar, D. (2013) Green Synthesis and Characterization of ZnS Nanoparticles. *Research Journal of Physical Sciences*, **1**, 1-6.

[4] Baishya, U. and Sarkar, D. (2011) ZnS Nanocomposite Formation: Effect of ZnS Source Concentration Ratio. *Indian Journal of Pure and Applied Physics*, **49**, 186-189.

[5] Maji, S.K., Mukherjee, N., Mondal, A., Adhikary, B. and Kamakar, B. (2011) Synthesis of Nanocrystalline and Mesoporous Zinc Sulphide from a Single Precursor $Zn(SOCCH_3)_2Lut_2$ Complex. *Journal of Physics and Chemistry of Solids*, **72**, 784-788. https://doi.org/10.1016/j.jpcs.2011.03.011

[6] Pathak, C.S., Mandal, M.K. and Agarwala, V. (2013) Synthesis and Characterization of Zinc Sulphide Nanoparticles Prepared by Mechanochemical Route. *Superlattices and Microstructues*, **58**, 135-143. https://doi.org/10.1016/j.spmi.2013.03.011

[7] Hoa, T.T.Q., Vu, L.V., Canh, T.D. and Long, N.N. (2009) Preparation of ZnS Nanoparticles by Hydrothermal Method. *Journal of Physics*: *Conference Series*, **187**, Article ID: 012081.

[8] Tan, W.B., Huang, N. and Zhang, Y. (2007) Ultrafine Biocompatible Chitosan Nanoparticles Encapsulating Multi-Coloured Quantum Dots for Bioapplications. *Journal of Colloid and Interface Science*, **310**, 464-470. https://doi.org/10.1016/j.jcis.2007.01.083

[9] Grobelsek, I., Rabung, B., Quilitz, M. and Veith, M. (2011) Electrochemical Synthesis of Nanocrystalline Zinc Oxide and Phase Transformations of Zinc Hydroxides. *Journal of Nanoparticle Research*, **13**, 5103-5119. https://doi.org/10.1007/s11051-011-0490-0

[10] Han, W.-K., Choi, J.-W., Hwang, G.-H., Hong, S.-J., Lee, J.-S. and Kang, S.-G. (2006) Fabrication of Cu Nano Particles by Direct Electrochemical Reduction from CuO Nano Particles. *Applied Surface Science*, **252**, 2832-2838. https://doi.org/10.1016/j.apsusc.2005.04.049

[11] Rodríguez-Sánchez, L., Blanco, M.C. and López-Quintela, M.A. (2000) Electrochemical Synthesis of Silver Nanoparticles. *The Journal of Physical Chemistry B*, **104**, 9683-9688. https://doi.org/10.1021/jp001761r

[12] Lide, D.R. (2007-2008) "Zirconium", CRC Handbook of Chemistry and Physics. CRC Press, New York, 42.

[13] Perk, L. (2009) The Future of Immune-PET in Drug Development Zirconium-89 and Iodine-124 as Key Factors in Molecular Imaging. Wayback Machine, Amsterdam.

[14] Ingelfinger, J.R. (2015) A New Era for the Treatment of Hyperkalemia? *New England Journal of Medicine*, **372**, 275-277. https://doi.org/10.1056/NEJMe1414112

[15] Vázquez-Cuchillo, O., Gómez, R., Cruz-López, A., Torres-Martínez, L.M., Zanella, R., Alejandre Sandoval, F.J. and Del Ángel-Sánchez, K. (2013) Improving Water Splitting Using $RuO_2$-Zr/$Na_2Ti_6O_{13}$ as a Photocatalyst. *Journal of Photochemistry and Photobiology A*: *Chemistry*, **266**, 6-11.

[16] Coudray, C., Rachidi, S. and Favier, A. (1993) Effect of Zinc on Superoxide-Dependent Hydroxyl Radical Production *in Vitro*. *Biological Trace Element Research*, **38**, 273-287.

[17] Subramani, A.K., Byrappa, K., Ananda, S., Lokanatha Rai, K.M., Ranganathaiah, C. and Yoshimura, M. (2007) Photocatalytic Degradation of Indigo Carmine Dye Using $TiO_2$ Impregnated Activated Carbon. *Bulletin of Materials Science*, **30**, 37-41.

[18] Lakshmi, G.C., Ananda, S., Somashekar, R. and Ranganathaiah, C. (2012) Synthesis of ZnO/$ZrO_2$ Nano Composites by Electrochemical Method and Its Application for

Photocatalytic Degradation of Fast Green FCF Dye and Paper Dyeing and Printing Press Effluents. *International Journal of Advanced Materials Sciences*, **3**, 221-237.

[19] Byrappa, K., Subramani, A.K., Ananda, S., Rai, K.M.L., Dinesh, R. and Yoshimura, M. (2006) Photocatalytic Degradation of Rhodamine B Dye Using Hydrothermally Synthesized ZnO. *Bulletin of Materials Science*, **29**, 433-438. https://doi.org/10.1007/BF02914073

[20] Neelakandeswaria, N., Sangamia, G., Dharmaraja, N., Taekb, N.K. and Kimb, H.Y. (2011) Spectroscopic Investigations on the Photodegradation of Toluidine Blue Dye Using Cadmium Sulphide Nanoparticles Prepared by a Novel Method. *Spectrochimica Acta Part A*, **78**, 1592-1598.

[21] Xue, Y., Luan, Q., Yang, D., Yao, X. and Zhou, K. (2011) Direct Evidence for Hydroxyl Radical Scavenging Activity of Cerium Oxide Nanoparticles. *The Journal of Physical Chemistry*, **115**, 4433-4438.

[22] Mohamed, S.H. (2010) Photocatalytic, Optical and Electrical Properties of Copper-Doped Zinc Sulfide Thin Films. *Journal of Physics D*: *Applied Physics*, **43**, Article ID: 035406. https://doi.org/10.1088/0022-3727/43/3/035406

[23] Li, C. and Song, G. (2009) Photocatalytic Degradation of Organic Pollutants and Detection of Chemical Oxygen Demand by Fluorescence Methods. *Sensors and Actuators B*: *Chemical*, **137**, 432-436. https://doi.org/10.1016/j.snb.2009.01.055

[24] Lakshmi, G.C., Ananda, S., Somashekar, R. and Ranganathiah, C. (2012) Synthesis, Characterization and Photocatalytic Activity of ZnO: Sn Nanocomposites. *International Journal of Advances Science and Technology*, **5**, 54-64.

[25] Van Dijken, A., Janssen, A.H., Smitsmans, M.H., Vanmaekelbergh, D. and Meijerink, A. (1998) Size-Selective Photoetching of Nanocrystalline Semiconductor Particles. *Chemistry of Materials*, **10**, 3513-3522. https://doi.org/10.1021/cm980715p

[26] Li, W., Li, D., Wang, J., Shao, Y., You, J. and Teng, F. (2013) Exploration of the Active Species in the Photocatalytic Degradation of Methyl Orange under UV Light Irradiation. *Journal of Molecular Catalysis A*: *Chemical*, **380**, 10-17. https://doi.org/10.1016/j.molcata.2013.09.001

[27] Li, H., Hong, W., Cui, Y., Jia, Q. and Fan, S. (2013) High Photocatalytic Activity of C-$ZnSn(OH)_6$ Catalysts Prepared by Hydrothermal Method. *Journal of Molecular Catalysis A*: *Chemical*, **378**, 164-173. https://doi.org/10.1016/j.molcata.2013.06.012

[28] Nešić, J., Manojlović, D.D., Anđelković, I., Dojčinović, B.P., Vulić, P.J., Krstić, J. and Roglić, G.M. (2013) Preparation, Characterization and Photocatalytic Activity of Lanthanum and Vanadium Co-Doped Mesoporous $TiO_2$ for Azo-Dye Degradation. *Journal of Molecular Catalysis A*: *Chemical*, **378**, 67-75.

[29] Nawawi, W.I. and Nawi, M.A. (2014) Carbon Coated Nitrogen Doped P25 for the Photocatalytic Removal of Organic Pollutants under Solar and Low Energy Visible Light Irradiations. *Journal of Molecular Catalysis A*: *Chemical*, **383**-**384**, 83-93. https://doi.org/10.1016/j.molcata.2013.11.030

[30] Sun, W.-J., Li, J., Mele, G., Zhang, Z.-Q. and Zhang, F.-X. (2013) Enhanced Photocatalytic Degradation of Rhodamine B by Surface Modification of ZnO with Copper (II) Porphyrin under Both UV-Vis and Visible Light Irradiation. *Journal of Molecular Catalysis A*: *Chemical*, **366**, 84-91.